



## Undoped and ytterbium-doped titanium aluminum nitride coatings for improved oxidation behavior of nuclear fuel cladding



Michael J. Brova<sup>a,c</sup>, Ece Alat<sup>a</sup>, Mark A. Pauley<sup>a,c</sup>, Rachel Sherbondy<sup>a,c</sup>, Arthur T. Motta<sup>a,b</sup>, Douglas E. Wolfe<sup>a,c,d,\*</sup>

<sup>a</sup> Department of Materials Science and Engineering, The Pennsylvania State University, University Park, PA 16802, USA

<sup>b</sup> Department of Mechanical and Nuclear Engineering, The Pennsylvania State University, University Park, PA 16802, USA

<sup>c</sup> Applied Research Laboratory, The Pennsylvania State University, 119 Materials Research Building, University Park, PA 16802, USA

<sup>d</sup> Department of Engineering Science and Mechanics, The Pennsylvania State University, University Park, PA 16802, USA

### ARTICLE INFO

#### Keywords:

Ceramic coating  
Nuclear fuel cladding  
Oxidation resistance  
Titanium aluminum nitride  
Reactive element effect  
Rare earth elements

### ABSTRACT

In an effort to develop coatings to increase the oxidation resistance of nuclear fuel cladding during a loss-of-coolant-accident (LOCA), undoped and ytterbium-doped titanium aluminum nitride ( $\text{Ti}_x\text{Al}_{1-x}\text{N}$ ) coatings were deposited onto ZIRLO® and grade-5 titanium substrates using a hybrid coating technique incorporating both resistance evaporation and cathodic arc physical vapor deposition (CA-PVD). The coating systems consisted of a titanium bond layer, an undoped TiAlN layer, and an outer TiAlN layer doped with varying levels of ytterbium (0.44 to 33.24 at.%). The coated materials were subjected to high temperature atmospheric oxidation testing and differential scanning calorimetry (DSC) to evaluate the effect of different Yb dopant concentrations on the  $\text{Ti}_x\text{Al}_{1-x}\text{N}$  coating oxidation resistance. The results showed that the coatings evaluated in this study protected the tubular ZIRLO® cladding material from oxidation when exposed to air at temperatures up to 1200 °C. DSC data showed that the corrosion resistance of coatings with Yb dopant concentrations of 0.44 and 0.64 at.% was better than that of undoped  $\text{Ti}_x\text{Al}_{1-x}\text{N}$  coatings and of  $\text{Ti}_x\text{Al}_{1-x}\text{N}$  coatings with Yb concentrations  $\geq 4.78$  at.%. Yb doping and the 0.44 and 0.64 at.% level also resulted in a lower rate of oxide scale growth and improved scale adherence, which further slowed oxidation kinetics. Peak oxidation resistance was observed in the TiAlN coating with a 0.44 at.% ytterbium dopant concentration. Ytterbium concentrations of 4.78 at.% and greater led to accelerated oxidation rates for the testing conditions studied compared to undoped TiAlN. These results show that ytterbium doped coatings are possible candidates for high temperature resistance of accident tolerant fuel coatings.

### 1. Introduction

Zirconium alloys are used in the nuclear industry for fuel rod cladding due to their low neutron absorption cross section, good mechanical properties, resistance to corrosion, high thermal conductivity, and generally long operational life span [1,2]. While these alloys perform adequately under normal operating conditions, they behave less well in the high temperature environment associated with a loss-of-coolant-accident (LOCA). In the case of a LOCA, the cladding temperature can reach upwards of 1200 °C, and the exposure of the cladding to steam and air results in the rapid formation of zirconium oxide and the production of hydrogen gas. The associated production of hydrogen can lead to the formation of combustible oxygen-hydrogen mixtures which can worsen a nuclear accident [2].

The realization of this vulnerability stemming from the Fukushima-

Daichii accident in 2011 has led to research into the development of nuclear fuel cladding material systems with improved performance during a design basis accident such as a LOCA or in the case of beyond design basis accidents. These so-called accident tolerant fuels (ATF) are evaluated based on their ability to provide additional coping time prior to nuclear fuel cladding failure in the case of an accident when compared to the standard zirconium-based fuel cladding. Many ATF concepts exist, some of which call for the replacement of the zirconium alloy based fuel cladding with other types of material (SiC, FeCrAl, etc.) [3]. As an alternative, the application of thin protective coatings to the current zirconium-based systems is attractive because these fuel rods would be compatible with current nuclear reactor designs, thereby minimizing implementation costs. The thin coatings option also minimize the ATF neutronic penalties.

In previous works, single layer TiN, single layer  $\text{Ti}_x\text{Al}_{1-x}\text{N}$ , and TiN/

\* Corresponding author at: Department of Materials Science and Engineering, The Pennsylvania State University, University Park, PA, 16802, USA.  
E-mail address: [dew125@psu.edu](mailto:dew125@psu.edu) (D.E. Wolfe).

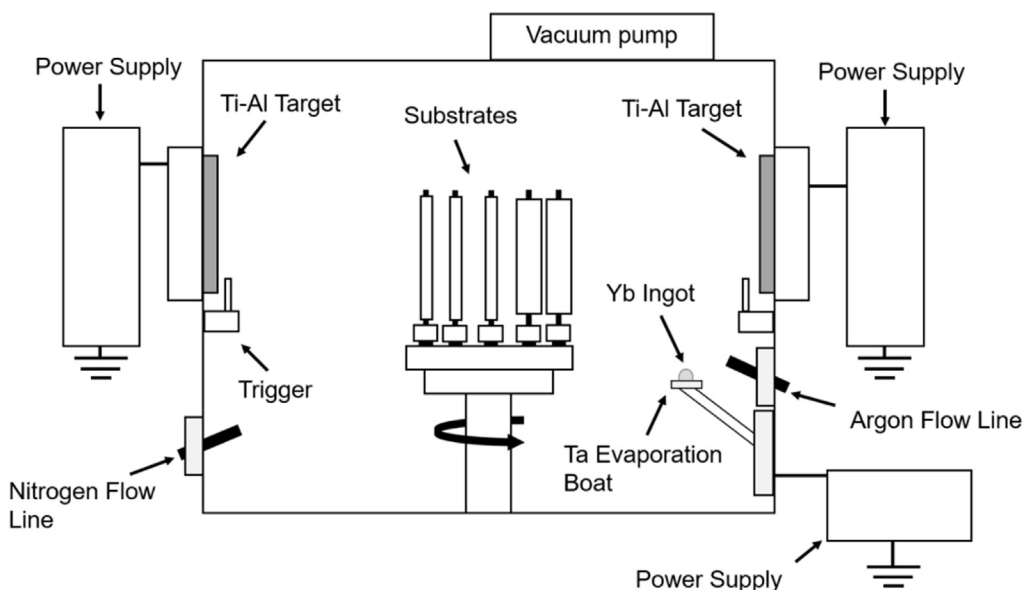


Fig. 1. Schematic of modified cathodic arc system used to deposit titanium aluminum nitride (TiAlN) coatings with ytterbium dopant (TiAlN + Yb) evaporated via resistance heating.

$\text{Ti}_x\text{Al}_{1-x}\text{N}$  multilayer coatings were deposited on Zircaloy-4 and ZIRLO® claddings by pulsed laser deposition (PLD) and cathodic arc physical vapor deposition (CA-PVD) [4–6] and evaluated for corrosion.<sup>1</sup> It has been shown that TiN, TiAlN, and TiN/ $\text{Ti}_x\text{Al}_{1-x}\text{N}$  coating systems on both Zircaloy-4 and ZIRLO® can substantially increase the corrosion resistance of nuclear fuel cladding during autoclave corrosion testing under simulated nuclear reactor conditions (for Zircaloy-4 deaerated water at 500 °C at 25 MPa and ZIRLO® in static pure water at 360 °C at 18.7 MPa) [4–5]. The question remained then of what their behavior would be during higher temperature corrosion testing. In the present study, titanium aluminum nitride coatings of composition  $\text{Ti}_x\text{Al}_{1-x}\text{N}$ , where  $x \sim 0.46\text{--}0.54$  at.%, and with varying ytterbium dopant concentrations were deposited on ZIRLO® substrates to investigate their ability to protect the substrate from high temperature oxidation. Such coatings are very hard, refractory, and oxidation resistant and have been used primarily in high-performance cutting and finishing tools [7,8]. While TiN oxidizes at 600 °C,  $\text{Ti}_x\text{Al}_{1-x}\text{N}$  oxidizes between 800 °C and 1000 °C, depending on composition. Upon oxidation, TiN tends to form a thin titania (rutile or anatase) oxide scale whereas TiAlN forms an alumina (preferably alpha alumina) protective barrier layer which reduces further oxidation of the coating [5,23]. The formation of the outer alumina layer improves the corrosion performance by several orders of magnitude relative to uncoated Zr alloys, as the diffusion coefficient of oxygen through aluminum oxide is much lower than through the native zirconium oxide layer of the cladding [10]. It has also been shown that aluminum rich  $\text{Ti}_x\text{Al}_{1-x}\text{N}$  coatings can provide protection upwards of 1200 °C depending on the composition and environmental conditions [7,9].

Rare-earth (RE) doping has been shown to further raise the oxidation temperature of the metallic alloys and coatings that produce  $\text{Al}_2\text{O}_3$  and  $\text{Cr}_2\text{O}_3$  passivation layers due to a phenomenon known as the reactive element effect (REE) [12]. For reasons that are not fully understood, the introduction of small concentrations of rare-earth elements has been shown to impede the outward cation diffusion during an oxidative process, which directly lowers the oxidation rate [11–16]. Additionally, the REE leads to a reduced number of voids along metal-scale interfaces for alloys doped with reactive elements (especially those containing sulfur impurities), which helps reduce oxide scale

spallation, again improving oxidation resistance [11–12]. Finally, the REE also leads to denser passivation scales with an overall smaller grain size [11,17]. For this study, ytterbium was chosen as the dopant species within the  $\text{Ti}_x\text{Al}_{1-x}\text{N}$  coating to further improve the protective nature of the  $\text{Ti}_x\text{Al}_{1-x}\text{N}$  coating on ZIRLO®. To the authors' knowledge, the Yb rare-earth effect has never been studied on  $\text{Ti}_x\text{Al}_{1-x}\text{N}$  systems for improving oxidation behavior of nuclear fuel cladding.

## 2. Experimental methods

### 2.1. Materials and coating

Undoped and Yb-doped  $\text{Ti}_x\text{Al}_{1-x}\text{N}$  (where  $x \sim 0.46\text{--}0.54$  at.%) coatings (henceforth referred to as TiAlN and TiAlN + Yb coatings, respectively) were deposited onto ZIRLO® coupons, ZIRLO® tubes, and grade-5 titanium rods. Both the ZIRLO® coupons and tubes were supplied by Westinghouse (Pittsburgh, PA) as sheet material and extruded tubular fuel cladding. The nominal composition of ZIRLO® is 1 wt.% Nb, 1 wt.% Sn, 0.1 wt.% Fe and balance Zr, and the composition of grade-5 titanium is 6 wt.% Al, 4 wt.% V, and balance Ti (Ti-6Al-4 V). The ZIRLO® sheet material was cut into 2.54 cm × 5.08 cm × 0.043 cm coupons. The interior diameter of the ZIRLO® tubes was 0.83 cm and the outer diameter was 0.95 cm. The tubes were cut into 3.94 cm-long sections. The diameter of the grade-5 titanium rods was 3.18 mm and the rods were cut into 7.62 cm-long sections. Prior to coating deposition, all substrates were hand ground using 320 grit SiC paper in order to remove defects produced during cutting, to round the edges, and to reduce potential stress-induced failure initiation sites. Green Scotch-Brite scouring pads were used to remove the zirconium-based native oxide and obtain the desired surface roughness ( $R_a$ ) value of 0.25 μm (10 microinch). After the grinding step, the substrates were cleaned in an ultrasonic bath of acetone for 10 min, cleaned in an ultrasonic bath of methanol for 10 min, rinsed with deionized water, and then dried with 99.999% nitrogen gas.

### 2.2. Coating deposition

The TiAlN + Yb coatings were deposited using a hybrid coating deposition technique (shown in Fig. 1) in which the Yb dopant was evaporated via resistance heating while a TiAl alloy target was simultaneously evaporated using cathodic arc physical vapor deposition (CA-PVD) in a nitrogen-rich plasma atmosphere. The CA-PVD technique was chosen to deposit the TiAlN layer because of its ability to produce coatings with high adhesion strength and high density, and because the

<sup>1</sup> ZIRLO is a registered trademark of the Westinghouse Electric LLC, its Affiliates and/or Subsidiaries in the United States of America and may be registered in other countries throughout the world. All rights reserved. Unauthorized use is strictly prohibited. Other names may be trademarks of their respective owners.

process can be easily scaled to commercial production volumes [4,8,18].

During the CA-PVD coating process, the TiAl “target”, or cathode, was positively biased compared to the rest of the system while the substrate (either ZIRLO® or Ti-6Al-4 V), or anode, was negatively biased. The evaporation of the target (TiAl) material occurs when a high-current, low-voltage arc is struck on the cathode (by way of a mechanical trigger device), which generates a small, yet energetic emitting zone referred to as the cathodic spot (on average 1 to 10  $\mu\text{m}$  in diameter). The current density of the cathode hot spot is between  $10^6$  and  $10^8$   $\text{A}/\text{cm}^2$ . Material is ionized and emitted from the cathode spot at velocities ranging from 10 to 1000  $\text{m}/\text{s}$  in plasma form, where it can react with gases in the deposition chamber environment [18,25–27]. Several cathodic spots function together to form a plasma plume which is directed towards the negatively biased substrate. As a result the substrate is bombarded with the reacted ions and these become the deposited coating.

The primary drawback of the reactive CA-PVD process is that macroparticles or microdroplets are emitted during the flash evaporation events at the cathode spots. Macroparticles are 0.1 to 10  $\mu\text{m}$  diameter particles that have a volume-to-surface area ratio that is too large for the particles to react completely with the gas present in the chamber. The result is that macroparticles are high in metal content (near the TiAl intermetallic target composition) relative to the desired coating stoichiometry. Macroparticles are of particular concern in applications for which the localized mechanical and adhesive weaknesses caused by the particles degrade the performance of the coating [8,18].

For the current study, a high purity titanium target (99.999%) and a specialty  $\text{Ti}_{0.33}\text{Al}_{0.67}$  (at.%) alloy target (99.99%) were purchased from Surface Engineering Group (Minnesota) for the titanium bond layer and  $\text{Ti}_x\text{Al}_{1-x}\text{N}$  layer depositions, respectively. The sputtering targets measured 6.35 cm in diameter by a depth of 3.56 cm. Miller XMT 304 CC/CV DC welder power supplies were used to evaporate the sputtering targets during coating deposition. The negative substrate bias was achieved using a 10 kW Advanced Energy MDX II DC power supply. Three ZIRLO® sheet samples, three ZIRLO® tube segments, one grade-5 titanium rod, and one zirconium rod were rotated counterclockwise at 6.75 rpm while mounted in a holder that also rotated counterclockwise but at 2.4 rpm. Since CA-PVD is a line-of-sight process, sample rotation is required to ensure coating thickness uniformity.

Resistive in situ thermal evaporation of ytterbium (obtained from HEFA Rare Earth, China) was used to dope the outer half of the TiAlN + Yb coatings. A M.A.P.S. EVP Series power supply ran high voltage through a high current transformer which fed the current through a customized thermal evaporation unit, as shown in Fig. 1. Ytterbium metal was placed in a tantalum evaporation boat to heat the Yb dopant species until evaporation at the desired rate was obtained. A nitrogen gas flow line at 17 sccm was used to direct the ytterbium vapor species to the samples during the deposition process.<sup>2</sup> Deposition parameters for the samples studied are listed in Table 1. The coating layers are TiAlN + Yb / TiAlN / Ti / ZIRLO® or Ti-6Al-4 V.

### 2.3. Evaluation and testing

The coated samples were analyzed using various characterization techniques including scanning electron microscopy (SEM), energy dispersive spectroscopy (EDS), electron probe microanalysis (EPMA), X-ray diffraction (XRD), optical microscopy (OM), and differential scanning calorimetry (DSC). Select samples were nickel-plated after

<sup>2</sup> It should be noted that a Yb concentration gradient does exist throughout the outer section of the  $\text{Ti}_x\text{Al}_{1-x}\text{N}$  coating due to the nature of the deposition method used. The coating's dopant concentration uniformity could be improved by using an alloyed target with the desired amount of Yb. For the current research program, however, the use of this method to produce coatings with the necessary range of REE dopant concentrations was cost prohibitive.

deposition to ensure coating edge retention during the grinding and polishing steps required for metallographic analysis. All cross-sectional thickness measurements of oxidized coatings were taken at several points across each sample, including regions in which coating spallation was observed. Prior to EPMA and EDS compositional data acquisition, the equipment was calibrated using Ti, Al, N, Yb, and Zr standards of known composition in order to ensure the fidelity of the measurements. All DSC thermographs were measured from room temperature to 1200 °C with a 10 °C/min heating rate and a 1-h isothermal hold in air [19].

For the furnace tests, a box furnace was heated to the desired oxidation temperature (1000–1200 °C). Samples were then inserted into the furnace which resulted in the maximum achievable heating rate (hundreds of degrees per minute). After the specified time (1.5, 4.0, 5.0, 6.0, 7.0, or 8.5 min), the samples were removed from the furnace and cooled in air to room temperature. Thermocouples placed in the vicinity of the samples were used to confirm that the samples reached 1200 °C within short time frames. However, the sample temperatures were not monitored when they were removed due to the fragility of the oxide layers that formed and to prevent the thermocouples from serving as a heat sink.

## 3. Results and discussion

### 3.1. Coating characterization

EPMA was used to measure the compositions of the TiAlN and TiAlN + Yb coatings as a function of distance through the coating thicknesses. Yb concentrations gleaned from these measurements have been plotted in Fig. 2g. It can be seen that significant variations in the Yb content through the thickness of each coating were observed. This variability is due to the designed initiation of the Yb evaporation halfway through the TiAlN depositions in addition to the variability of the evaporation process used for Yb deposition. For simplicity, analysis and identification of TiAlN and TiAlN + Yb samples, henceforth, will be conducted based on the maximum Yb concentration measured in each sample. These maximum Yb concentrations were found to be 0.00, 0.44, 0.64, 4.78, 19.72, and 33.24 at.%.

Backscattered electron SEM micrographs of polished TiAlN and TiAlN + Yb coating cross sections are shown in Fig. 2a-f. These SEM micrographs show the various layers within the coating systems including the ZIRLO® substrate, 0.6  $\mu\text{m}$  titanium bond layer, TiAlN, and TiAlN + Yb regions of the coating. In all TiAlN + Yb coatings, with the exception of the sample with 0.64 at.% Yb, a bright band can be seen approximately halfway through the TiAlN + Yb coating thickness, which corresponds to the location of the peak ytterbium dopant concentration. The dopant evaporation was started halfway through the TiAlN coating depositions, which matches well with the observed results. In the case of the 0.64 at.% Yb sample, it was not possible to control the ytterbium plasma initially. As a result, the energy and size of the plasma grew steadily as the evaporation current was increased. The bright region in the SEM micrograph is therefore located slightly above the coating midpoint. In all TiAlN + Yb coating depositions, the ytterbium plasma generated a distinct green color that could be monitored from the viewport of the deposition chamber. The intensity of this plume decreased with increasing deposition time, suggesting a gradual decrease in Yb co-evaporation, which was confirmed with EPMA (Fig. 2g). This observation corresponds with what is seen in the SEM micrographs as the regions above the bright ytterbium-rich bands appear slightly brighter than the undoped layer. This is especially apparent in coatings with higher Yb content (19.72 and 33.24 at.%).

In order to investigate the effect of ytterbium dopant concentration on the crystal structure of TiAlN + Yb coatings, X-ray diffraction was performed on the coated and uncoated flat ZIRLO® specimens. Fig. 3 shows the Bragg-Brentano patterns of the uncoated ZIRLO®, undoped TiAlN, and TiAlN + Yb coatings and glancing incidence (incidence

**Table 1**  
Parameters used for undoped and Yb doped TiAlN coating depositions.

Deposition time Ti/TiAlN/ TiAlN + Yb, (min)	Substrate bias Ti/TiAlN/ TiAlN + Yb (Volts)	Source Current Ti/ TiAlN/TiAlN + Yb (Amps)	Heater Temperature (°C)	Current through Yb (Amp)	Yb Plasma evaporation (min)	Yb at.% within Ti <sub>x</sub> Al <sub>1-x</sub> N
8/200/0	8/240/0	65/45/0	325	0	0	0
8/120/120	150/50/50	65/45/50	325	170	30	0.44
8/60/180	150/50/50	65/45/45	325	116	180	0.64
8/120/120	150/50/50	65/45/45	325	165	66	4.78
8/120/120	150/50/50	65/45/50	325	180	120	19.72
8/120/120	150/50/50	65/45/45	325	200	120	33.24

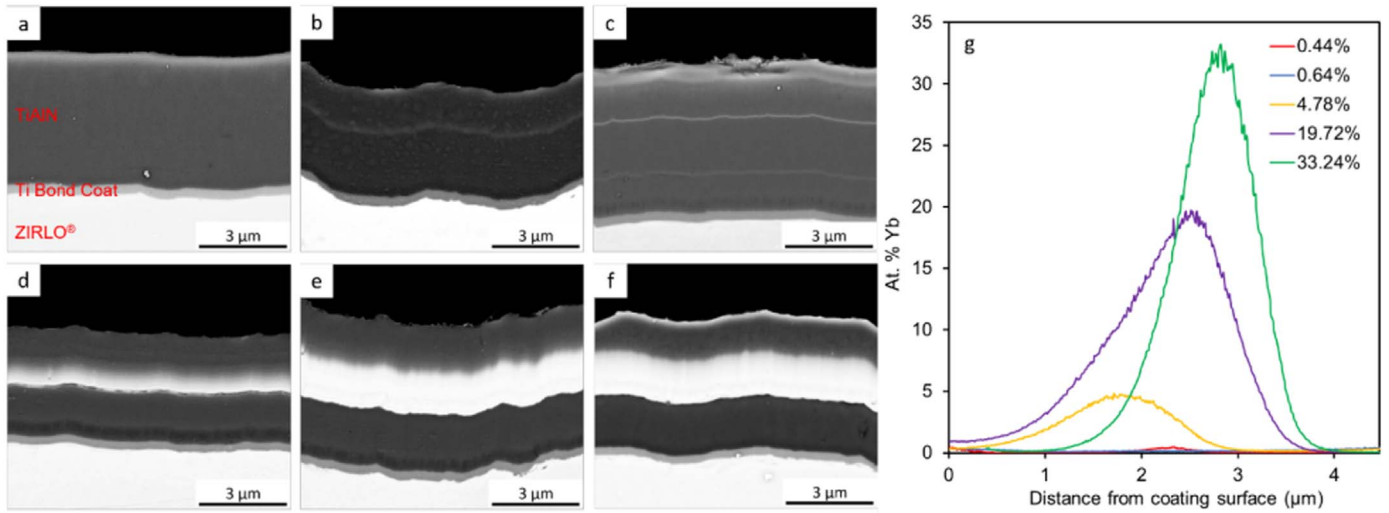


**Fig. 2.** Backscattered-electron SEM micrographs of as-deposited TiAlN and TiAlN + Yb coatings with maximum Yb concentrations: (a) 0.00 at.% Yb, (b) 0.44 at.% Yb, (c) 0.64 at.% Yb, (d) 4.78 at.% Yb, (e) 19.72 at.% Yb, and (f) 33.24 at.% Yb deposited on ZIRLO® substrates with a 0.6 µm titanium bond layer. The Yb at.% listed is the maximum Yb concentration detected by electron probe microanalysis (EPMA). All the coatings show bright bands that indicate ytterbium rich regions. (g) EPMA measurements showing Yb concentration distribution through coating thickness.

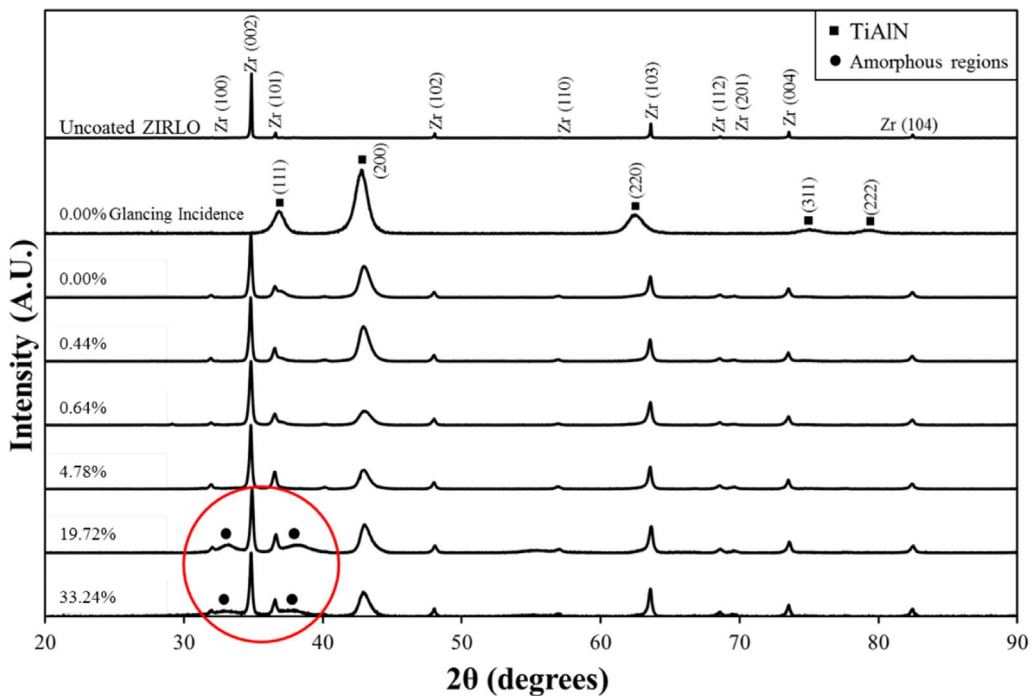


**Fig. 3.** Bragg brentano (Cu Kα) XRD patterns for uncoated ZIRLO®, TiAlN, TiAlN + Yb with 0.44, 0.64, 4.78, 19.72, and 33.24 at.% Yb., and glancing incidence (Cu Kα) XRD with (incidence angle = 1°) for TiAlN. Coatings with higher maximum Yb dopant concentrations (19.72 at.% and 33.24 at.%) showed the formation of an amorphous (red circle) phase which may explain the high temperature oxidation instability at 1200 °C. No ytterbium compounds/phases were observed in the XRD patterns. (For interpretation of the references to color in this figure legend, the reader is referred to the web version of this article.)

angle = 1°) XRD (Cu K $\alpha$ ) pattern for TiAlN deposited on ZIRLO® flat coupons. Both Bragg-Brentano and glancing incidence XRD patterns were utilized in order to differentiate between the substrate and TiAlN coating as several of the high intensity peaks overlapped. The crystal structure of the TiAlN coatings with the four lowest Yb concentrations (0.00, 0.44, 0.64, and 4.78 at.%) was determined to be cubic, matching ICDD card number 04–005-5251. The peaks observed during examination of the uncoated ZIRLO® approximately match the hexagonal crystal structure and card number 00–005-0665. Since these are coatings and not powders, variation in the peak position as well as in relative peak intensity was observed for the TiAlN coatings compared to the various ICDD diffraction database card patterns. While the samples with the four lowest Yb concentrations (0.00, 0.44, 0.64, and 4.78 at.%) all exhibited the cubic crystal structure within the TiAlN + Yb coating region, the higher Yb concentrations (19.72 and 33.24 at.%) showed evidence of broad peaks which suggest the presence of an amorphous phase. Since the Yb ionic radius (0.104 nm) is significantly larger than that of titanium (0.067 nm) and aluminum (0.053 nm), significant disruption in the lattice periodicity may have occurred to accommodate the high Yb concentrations, resulting in amorphous regions. The Yb-rich amorphous phase does not provide increased oxidation resistance compared to aluminum oxide or titanium oxide, and thus, resulted in poor resistance to oxidation for higher Yb concentrations (19.72 and 33.24 at.%). High resolution transmission electron microscopy could be performed to better understand the change in crystal structure with increasing ytterbium content in order to confirm the effect of excess Yb doping within the TiAlN coating system and to determine the size and volume fraction of the amorphous regions. The red circle in Fig. 3 shows the region in the diffraction patterns where the two amorphous peaks are present in the higher Yb concentration samples. We note that this amorphous phase differs from the wurtzite aluminum nitride phase that was previously found in as-deposited TiAlN coatings with sufficiently high yttrium dopant concentrations [20].

### 3.2. Furnace testing of coated grade-5 titanium

In order to isolate the effect of ytterbium dopant concentration on the oxidation behavior of TiAlN, static oxidation testing was performed on coated grade-5 titanium rods. Grade-5 titanium was chosen because it has the same crystal structure as ZIRLO® (HCP crystal structure), and because it oxidizes at a lower rate than ZIRLO® in oxygen-rich environments [21]. After atmospheric oxidation testing for times ranging from 1.5–8.5 min, the samples were removed from the furnace and allowed to cool before being prepared for cross-sectional metallographic analysis in order to determine the oxide layer thicknesses. Fig. 4 shows scanning electron micrographs of the polished cross-sections of undoped TiAlN on a grade-5 titanium substrate after furnace testing at 1200 °C for 4.0, 5.0, 6.0, 7.0, and 8.5 min in air. As expected, the oxide layer thickness increased with exposure time. For exposure times shorter than 1.5 min at 1200 °C (not shown), little to no oxide layer thickness was observed via backscattered SEM. This is likely because the sample temperature lagged slightly in reaching the 1200 °C furnace temperature (i.e., time is needed to equilibrate the sample temperature with the furnace temperature). Varying levels of brightness can be seen within the oxide layers of all analyzed samples suggesting that the composition of the oxide scales is not uniform. It was found through EDS mapping that the darker regions within the oxide were rich in aluminum, while the regions appearing bright were rich in titanium. A thin aluminum oxide layer was expected to grow on the outermost surface of the coating, which would offer optimal protection to the underlying TiAlN layer. However, as observed in Fig. 4, a mixed oxide phase of titanium oxide (bright regions) and aluminum oxide (dark regions) is observed throughout the oxide layer. The existence of mixed oxide regions, as opposed to separate oxide layers of alumina (outer) and titania (inner), is most likely a result of the nanocomposite structure of the TiAlN composition used and of the high heating rates

used for the oxidation testing. Future studies have been planned to investigate the oxide layer thickness growth rate and phase formation as a function of heating rate, time, and temperature to determine optimal alpha alumina outer layer formation conditions.

Fig. 5 shows the coating recession rates of TiAlN and TiAlN + Yb during the 1200 °C air oxidation testing of all coatings from 1.5 to 8.5 min exposure time. The coating recession rate was defined as the change in the thickness of the nitride portion of the coating with respect to time while at temperature during an oxidative process. This recession rate was found by fitting a linear regression model to the evolution of the measured coating thicknesses with time at elevated temperature with the slope representing the recession rate. The undoped coating was found to have a recession rate of 1.01  $\mu\text{m}/\text{min}$  and the coatings with Yb concentrations of 0.44 and 0.64 at.% receded at rates of 0.82 and 0.85  $\mu\text{m}/\text{min}$ , respectively. The lower recession rates of the coatings doped with 0.44 and 0.64 at.% Yb compared to the undoped baseline (recession rate decrease of 20% and 17%, respectively) suggest that Yb dopant additions can improve the oxidation performance of TiAlN coatings if the dopant concentration is sufficiently small. As the dopant concentration was increased to 4.78 at.%, the coating recession rate (1.17  $\mu\text{m}/\text{min}$ ) was found to be higher than that of the undoped baseline sample (1.01  $\mu\text{m}/\text{min}$ ), which suggests that too much Yb-dopant can result in lower oxidation resistance. Increasing the dopant concentration to 19.72 and 33.24 at.% resulted in large increases in the coating recession rate, i.e., increased coating oxidation which is attributed to the formation of the amorphous phase. It is possible that this decrease in oxidation resistance results from the amorphous regions not being as dense and protective as a thin layer of alpha alumina or titania (rutile/anatase), as has been demonstrated by J. Klöwer (2000) [22]. The ytterbium is also believed to lower the surface energy of adhesion which results in a more adherent oxide scale, but further investigation would be needed to confirm this possibility. The dependence of coating oxidation on Yb dopant concentration is similar to what has been shown with yttrium-doped titanium aluminum nitride, where small dopant concentrations improve the coating performance and larger concentrations are deleterious to the oxidation behavior [22].

An additional metric used to compare the effect of the doping species was the measurement of the oxide scale thickness as a function of time at elevated temperature. Fig. 6 shows the oxide scale thickness in microns as a function of time for TiAlN and TiAlN + Yb coatings with 0.0, 0.44, and 0.64 at.% Yb after atmospheric furnace testing at 1200 °C. The samples evaluated with dopant concentrations above 0.64 at.% Yb were found to form oxide scales which were not as adherent or durable as those produced by the samples with lower dopant concentrations. Therefore, coatings with 4.78, 19.72, and 33.24 at.% Yb were omitted as the high degree of oxide layer spallation and chipping resulted in oxide thickness measurements which failed to adequately represent the actual rate of oxide growth. A linear regression was fitted to the relationship between oxide layer thickness and time at temperature for each Yb dopant concentration tested. It can again be seen that the coating with 0.44 at.% Yb outperformed the 0.64 at.% Yb sample and both dopant compositions outperform the undoped TiAlN coating. The oxide layer thicknesses measured after the 6 min oxidation test for all compositions tested was found to exceed those predicted by the linear regression models. The source of the accelerated oxide growth rate observed at 6 min is unknown, but it may be related to the specific section of the coated rod where this specimen was removed, which may not have been as dense as other regions due to shadowing of the sample fixture. Further investigation is needed to determine the exact source of the variation in the rate of coating oxidation. Small concentrations of ytterbium led to a decrease in oxide layer thickness which is believed to be the result of the reactive element effect, which has been shown to promote the growth of denser oxide scales [17]. While the exact mechanism for the reactive element effect is still a point of discussion, the decrease in oxidation due to the addition of ytterbium (up to 0.64 at.% within the TiAlN coating) was

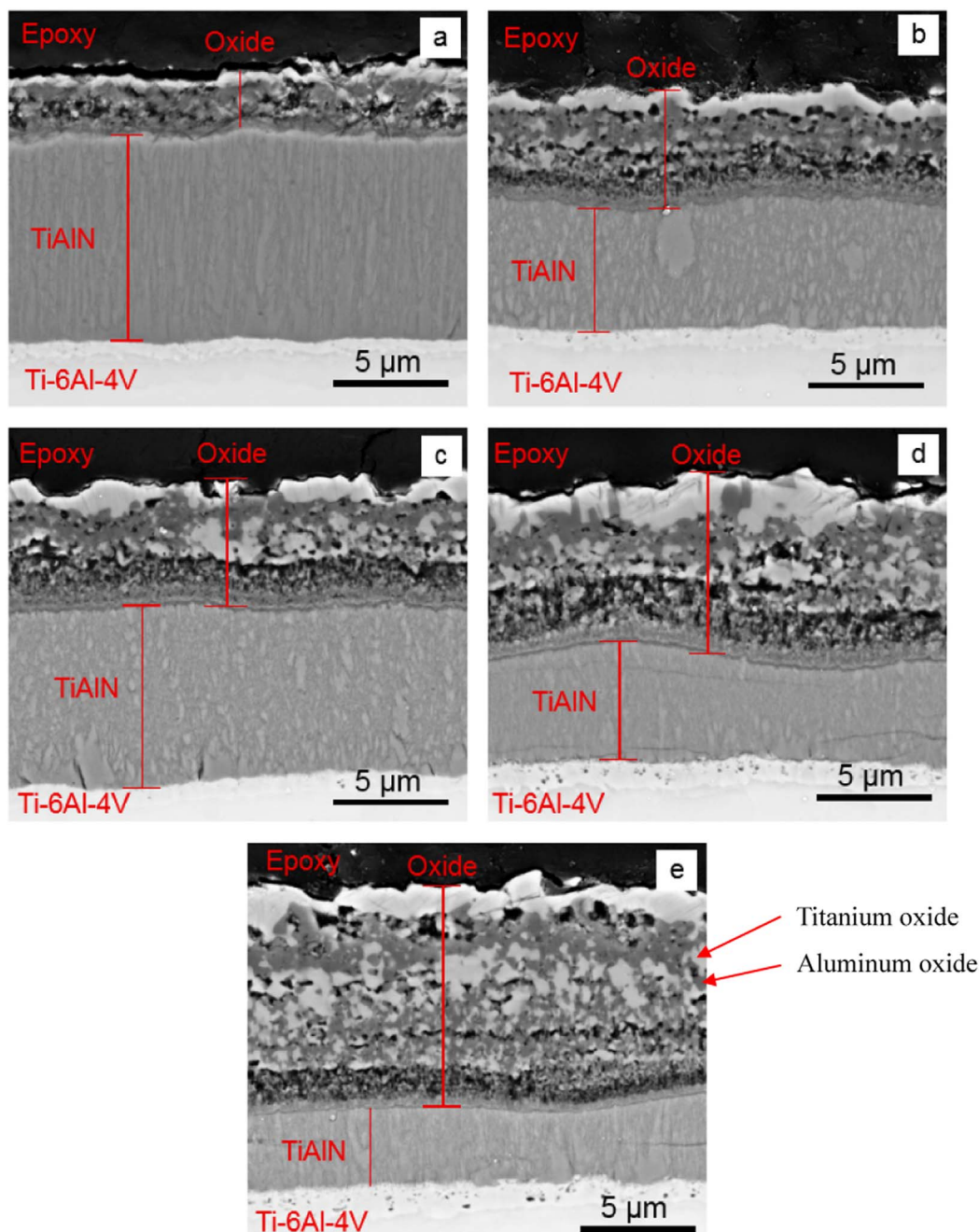


Fig. 4. Backscattered-electron SEM micrographs of undoped TiAlN on Ti-6-4 rod after oxidation at 1200 °C in air for (a) 4.0 min, (b) 5.0 min, (c) 6.0 min, (d) 7.0 min, and (e) 8.5 min.

similar to what was observed when Nd, Lu, and Y were used as dopants in order to improve the adhesion of  $\text{Al}_2\text{O}_3$  oxide scales to MCrAlY structural alloys [11].

### 3.3. Thermal analysis of ZIRLO® sheet

Differential scanning calorimetry (DSC) was used to identify phase transformations and the oxidation temperature of the coated system. Fig. 7 shows a differential scanning calorimetry thermograph, in which heat flow is plotted as a function of time (min), for the different Yb-doped titanium aluminum nitride coatings deposited on ZIRLO® sheet. Fig. 7 also shows the change in enthalpy of uncoated ZIRLO® oxidation during the same test. At a 10 °C/min heating rate, the exothermic peaks that occur between 145 and 160 min or 728 °C and 818 °C correspond to the temperatures at which the coating began to experience increased

oxidation. The large peaks that occur after 185 min or 943 °C correspond to the exothermic peak associated with the energy released due to the ZIRLO® oxidation. The curves show a shift downward as the test duration progressed due to the increasing mass of the samples (i.e., oxidation of the substrate and/or coating). The shape of the oxidation peaks observed in Fig. 7 changed based on the amount of ytterbium dopant. Low ytterbium dopant concentrations in the samples with 0.44 at.% and 0.64 at.% Yb appeared to shift the oxidation peaks to the right, corresponding to a delay in the time of oxidation. This delay is attributed to the low ytterbium concentrations acting to improve the oxide scale adherence and decrease to the oxidation rate. Once the oxide scale spalls, the exposed, uncoated substrate would rapidly oxidize and the process repeats. The oxidation temperature was determined by finding the intersection of tangent lines between the oxidation peak and the rest of the curve for each of the samples [24]. The maximum oxidative

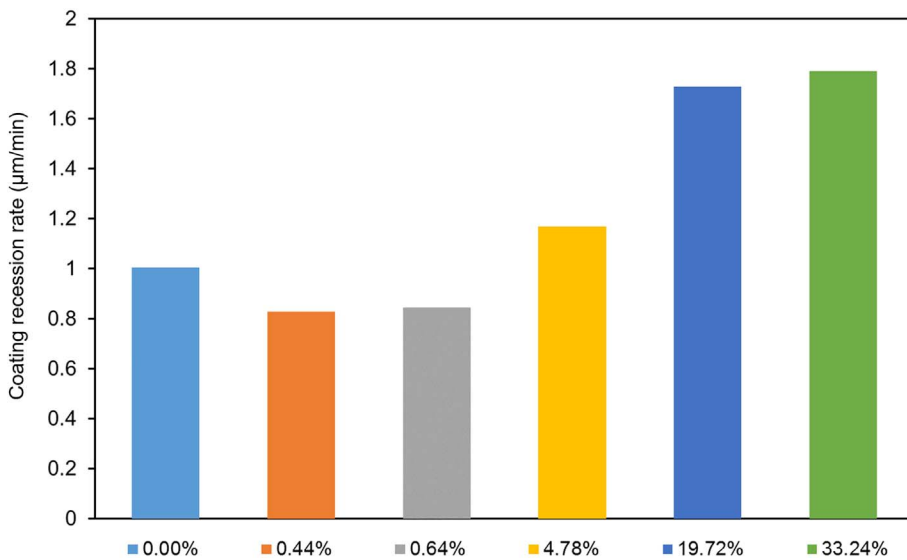


Fig. 5. TiAlN and TiAlN + Yb coating recession rates for 0.00, 0.44, 0.64, 4.78, 19.72, and 33.24 at.% Yb. calculated from atmospheric oxidation tests at 1200 °C for 1.5 to 8.5 min.

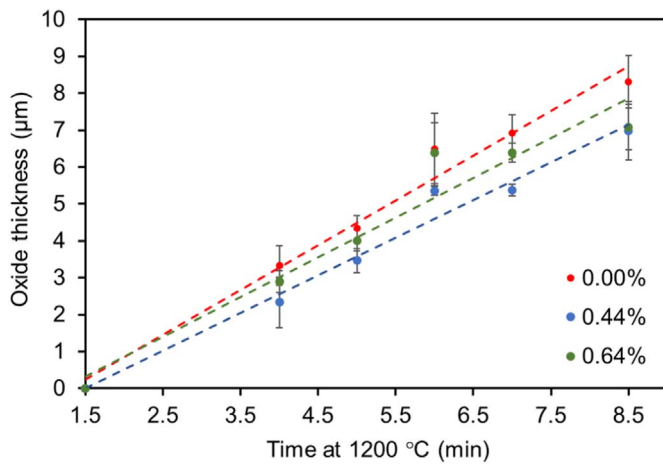


Fig. 6. Oxide thickness as a function of oxidation testing time at 1200 °C for TiAlN and TiAlN + Yb coatings with 0.00, 0.44, and 0.64 at.% Yb.

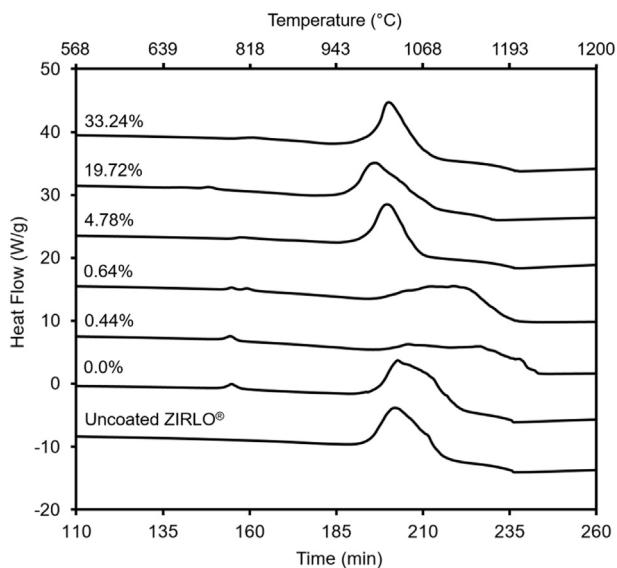


Fig. 7. DSC thermographs for TiAlN and TiAlN + Yb coatings with 0.00, 0.44, 0.64, 4.78, 19.72, and 33.24 at.% Yb on ZIRLO® flat substrates with a ramp rate of 10 °C/min from room temperature to 1200 °C with a 1 h isothermal hold at temperature.

behavior is observed at 978 °C (192 min). During sample preparation for DSC, the four edges of the sample were left uncoated, exposing the underlying substrate. These unexposed edges served as fast oxidation channels beneath the coated surface. If coated samples could be prepared with the entire substrate encapsulated, the distinction between the uncoated ZIRLO®, TiAlN coated, and TiAlN + Yb coatings would likely be improved.

Improved oxidation behavior was either significantly reduced or not observed in the elevated dopant concentration samples. This is attributed to the poor oxidative properties of ytterbium oxide compounds. The samples with 0.44 and 0.64 at.% Yb both had lower concentrations of ytterbium and outperformed all other coatings in the furnace testing. The best performing coating layer, both in terms of coating recession rate and oxide growth rate, was the sample with 0.44 at.% Yb. DSC testing of the 0.44 at.% Yb and 0.64 at.% Yb samples showed changes to their oxidation peak areas and temperatures suggesting a delayed onset of substrate oxidation shifted to higher temperatures compared with the uncoated ZIRLO® and undoped TiAlN. This suggests that undoped and doped TiAlN coatings offer additional oxidation protection for ZIRLO®. The higher temperature tail of the substrate peak of the sample with the 0.64 at.% Yb coating occurred at approximately 1198 °C or 236 min into the test. The undoped sample showed the end of the oxidation peak occurring at approximately 1126 °C or 222 min. This would correspond to a delay in the oxidation behavior of about 72 °C, which could be attributed to the oxide scale being more adherent for this sample compared to the others. The sample with 0.44 at.% Yb again showed improved performance as the peak was further broadened such that it ended at 243 min or 7 min past the time when the isothermal hold at 1200 °C was initiated. The oxidation peak in the 0.64 at.% Yb sample is split into two peaks which may be the result of defects within the coating. Although the DSC data suggests improved performance of the TiAlN undoped and doped coatings relative to the uncoated material, quantitative assessment is difficult due to the large relative volume of the base ZIRLO® compared to the volume of the TiAlN coating.

### 3.4. Atmospheric furnace testing of ZIRLO® tubes

Static oxidation testing was performed on coated ZIRLO® tubes which were subsequently cross sectioned. Analysis by Münz and Pflumm focused on the oxidation behavior of TiN coatings, AlN coatings, TiAlN coatings, and  $\gamma$ -TiAl intermetallics [23–24]. TiAlN was shown to oxidize at a rate of 400 µg/cm<sup>2</sup> after 1-h exposure to air at 1000 °C suggesting good performance [23–24]. For the current study, weight gain analysis would have been ideal to report the oxidation

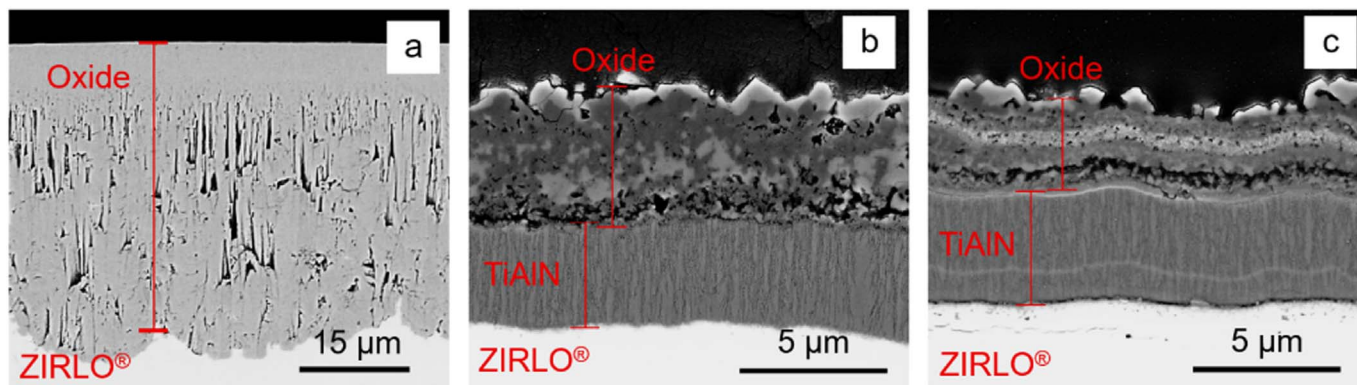


Fig. 8. Backscattered-electron SEM micrographs after isothermal oxidation testing at 1000 °C for 25 min for (a) uncoated ZIRLO® tube, (b) TiAlN deposited on a ZIRLO® tube, and (c) 0.64 at.% Yb.

behavior, but the exposed edges of the ZIRLO® samples would have incorrectly accelerated the observed rate of weight gain for coated samples. Instead, cross sectional microscopy was used to compare the oxide layer thickness for uncoated and coated samples. These preliminary results suggest that ytterbium and rare earth dopants in general can be used to enhance the corrosion resistant properties of TiAlN. Fig. 8 shows SEM micrographs of polished cross sectional samples comparing an uncoated ZIRLO® tube (Fig. 8(a)), (undoped) TiAlN deposited on a ZIRLO® tube Fig. 8 (b), and (0.64 at.% Yb) doped TiAlN deposited on a ZIRLO® tube after oxidation testing in air at 1000 °C for 25 min, Fig. 8(c). The uncoated ZIRLO® tube developed a 38.6 μm zirconium oxide (zirconia layer) that was not as uniform compared with the zirconia layer grown at 1200 °C for 4 min. The undoped and 0.64 at.% Yb samples developed 4.0 (± 0.5) and 3.1 (± 0.4) μm oxide scales respectively. Additionally, the undoped sample recessed to 68.4% of its original thickness, while the 0.64 at.% Yb sample recessed to 54.4% of its original thickness. In this instance, the coating with the ytterbium dopants of 0.64 at.% outperformed the undoped coating by 14.0% while both coatings acted to significantly reduce the oxidation of the uncoated ZIRLO® tube by almost an order of magnitude. At the current oxidation rate, the 0.64 at.% Yb doped coated sample protected the ZIRLO® for a further 21.0 min compared to the undoped sample for a total of 46.0 min of protection compared to the uncoated sample. This also suggests that the oxidation rate of the coating could be further reduced by a substantial degree if low concentrations of ytterbium were evenly distributed throughout the entire coating instead of existing in bands in the upper coating regime. This is also the first study to show that TiAlN can protect ZIRLO® in atmospheric oxidation testing at elevated temperatures. Extended oxidation protection could be further achieved by using thicker TiAlN coatings.

#### Conclusions and Future Work.

In order to improve the resistance of nuclear fuel cladding to high temperature oxidation, this study explored the effect of TiAlN and TiAlN + Yb coatings deposited on ZIRLO® substrates by a hybrid deposition technique utilizing resistance evaporation and cathodic arc physical vapor deposition. TiAlN and TiAlN + Yb coatings were deposited with ytterbium dopant concentrations of 0.00, 0.44, 0.64, 4.78, 19.72, and 33.24 at.% generated by in-situ thermal evaporation. TiAlN coatings were shown to reduce the rate of oxidation by over an order of magnitude compared to uncoated ZIRLO® during isothermal oxidation testing at 1100 °C. In addition, Yb dopant concentrations of 0.44 and 0.64 at.% were found to reduce the rate of TiAlN coating oxidation by ~20% compared to the undoped TiAlN coating when oxidized at 1200 °C. The improvement of the oxidation resistance observed resulting from Yb dopant additions has been attributed to the REE. The REE is believed to slow oxide growth kinetics through the diffusion of rare earth elements to grain boundaries resulting in slowed cation diffusion and grain size reduction due to solute-drag induced reductions in

grain boundary mobility. At higher dopant concentrations ( $\geq 4.78$  at.% Yb), the oxidation performance of the TiAlN + Yb coatings was drastically reduced when compared to undoped TiAlN. The deleterious nature of sufficiently high levels of Yb for the conditions studied is believed to be due to the formation of nonproductive reactive element oxides which increase the rate of oxygen diffusion through the oxide scale.

The results show that, TiAlN coatings with or without rare earth element dopants have the potential to be an effective means by which to improve the accident tolerance of zirconium nuclear fuel cladding. Further work focused on evaluating these systems under different time, temperature, humidity, and irradiation testing parameters could be conducted to confirm their viability for use in industrial applications. Additionally, CA-PVD depositions with the use of TiAl targets doped with various Yb concentrations should be used to conduct a more rigorous evaluation of the effect of Yb dopants on the oxidation performance of TiAlN coatings.

#### Acknowledgements

This research was sponsored by the U.S. Department of Energy, Office of Nuclear Energy, Nuclear Engineering University Programs (NEUP), under grant number DE-AC07-05ID14517.

#### References

- [1] M. Steinbrück, M. Böttcher, Air oxidation of Zircaloy-4, M5® and ZIRLO™ cladding alloys at high temperatures, *J. Nucl. Mater.* 414 (2011) 276–285.
- [2] T.R. Allen, R.J.M. Konings, A.T. Motta, *Comprehensive Nuclear Mater*, first ed, Elsevier Ltd., Amsterdam, 2012, pp. 49–68.
- [3] L. Hallstadius, S. Johnson, E. Lahoda, Progress in Nuclear Energy Cladding for high performance fuel, *Prog. Nucl. Energy* 57 (2012) 71–76.
- [4] E. Alat, A.T. Motta, R.J. Comstock, J.M. Partezana, D.E. Wolfe, Ceramic coating for corrosion (c3) resistance of nuclear fuel cladding, *Surf. Coat. Technol.* 281 (2015) 133–143.
- [5] F. Khatkhatay, L. Jiao, J. Jian, W. Zhang, Z. Jiao, J. Gan, H. Zhang, X. Zhang, H. Wang, Superior corrosion resistance properties of TiN-based coatings on Zircaloy tubes in supercritical water, *J. Nucl. Mater.* 451 (2014) 346–351.
- [6] E. Alat, A.T. Motta, R.J. Comstock, J.M. Partezana, D.E. Wolfe, Multilayer (TiN, TiAlN) ceramic coatings for nuclear fuel cladding, *J. Nucl. Mater.* 478 (2016) 236–244.
- [7] T. Leyendecker, O. Lemmer, S. Esser, J. Eberink, The development of the PVD coating TiAlN as a commercial coating for cutting tools, *Surf. Coat. Technol.* 48 (1991) 175–178.
- [8] B. M. Gabriel, Synthesis-structure-property-performance relationships of TiN, CrN, and nanolayer (Ti,Cr)N coatings deposited by cathodic arc evaporation for hard particle erosion, 2009.
- [9] A. Rahmel, M. Schütze, W.J. Quadackers, Fundamentals of TiAl oxidation - A critical review, *Mater. and Corros.* 46 (1995) 271–285.
- [10] P. N. L. E.L. Courtright, J.t. Prater, C.H. Henager, E.N. Greenwell, Oxygen Permeability for Selected Ceramic Oxides in the Range 1200–1700, Pac. Northwest Lab., Richland Washington, 1991.
- [11] A. Heuer, On the growth of Al<sub>2</sub>O<sub>3</sub> scales, *Acta Mater.* 61 (2013) 6670–6683.
- [12] B.A. Pint, Experimental Observations in Support of the Dynamic-Segregation Theory to Explain the Reactive-Element Effect, *Oxid. Met.* 45 (1996) 1–37.

- [13] B.A. Pint, Optimization of Reactive-Element Additions to Improve Oxidation Performance of Alumina-Forming Alloys, *J. Am. Ceram. Soc.* 86 (2003) 686–695.
- [14] F. Rovere, P.H. Mayrhofer, A. Reinholdt, J. Mayer, J.M. Schneider, The effect of yttrium incorporation on the oxidation resistance of Cr-Al-N coatings, *Surf. Coat. Technol.* 202 (2008) 5870–5875.
- [15] W. T. G., L. B. Pfeil, Improvement in Heat Resistant Alloys, 459848, 1937.
- [16] A. Ul-Hamid, T.E.M. Study, of the Effect of Y on the Scale Microstructures of Cr<sub>2</sub>O<sub>3</sub> - and Al<sub>2</sub>O<sub>3</sub> - Forming Alloys, *Oxid. Met.* 58 (2002) 23–40.
- [17] B.A. Pint, Progress in understanding the reactive element effect since the Whittle and Stringer literature review, Oak Ridge National, Laboratory (2001).
- [18] H. Randhawa, Cathodic Arc Plasma Deposition Technology, *Thin Solid Films* 167 (1988) 175–185.
- [19] P. Gabbott, A Practical Introduction to Differential Scanning Calorimetry, Principles and Applications of Thermal Analysis, Blackwell Pub. Ltd., New Jersey, 2008, pp. 1–50.
- [20] M. Moser, P.H. Mayrhofer, Yttrium-induced structural changes in sputtered Ti<sub>1-x</sub>Al<sub>x</sub>N thin films, *Scr. Mater.* 57 (2007) 357–360.
- [21] V.I. D'yachkov, High-Temperature Oxidation of Titanium, Zirconium, and Hafnium in Steam, *Russian J. of Appl. Chem.* 79 (2006) 908–913.
- [22] J. Klöwer, Factors affecting the oxidation behaviour of thin Fe-Cr-Al foils Part II: The effect of alloying elements: Overdoping, *Mater. Corros.* 51 (2000) 373–385.
- [23] W.D. Münz, Titanium aluminum nitride films, A new alternative to TiN coatings, *J. of Vac. Science & Technol. A: Vac., Surf., and Films* 4 (6) (1986) 2717–2725.
- [24] R. Pflumm, et al., Oxidation protection of  $\gamma$ -TiAl-based alloys-A review, *Intermetallics* 56 (2015) 1–14.
- [25] Michael W. Reedy, Brian M. Gabriel, Douglas E. Wolfe, Erosion Performance and Characterization of Nanolayer (Ti,Cr)N Hard Coatings for Gas Turbine Engine Compressor Blade Applications, *Surf. and Coat. Technol.* 206, (2011) 464–472.
- [26] B. Borawski, J. Singh, J.A. Todd, D.E. Wolfe, Multilayer coating design architecture for optimum particulate erosion resistance, *J. of Wear* 271 (2011) 2782–2792.
- [27] B. Borawski, J.A. Todd, D.E. Wolfe, The influence of ductile interlayer material on the particle erosion resistance of multilayered TiN based coatings, *J. of Wear* 271 (2011) 2890–2898.